ChemPubSoc Europe

DOI: 10.1002/cctc.201300399

Electrosteric Activation by using Ion-Tagged Prolines: A Combined Experimental and Computational Investigation

Andrea Bottoni,[a] Marco Lombardo,*[a] Gian Pietro Miscione,*[a] Elisa Montroni,[a, b] Arianna Quintavalla,[a] and Claudio Trombini[a]

We have recently proposed the empirical concept of electrosteric activation to explain the improved catalytic performances observed for a series of ion-tagged catalysts compared to the parent tag-free structures. Here, the results of a combined experimental and computational investigation on the asymmetric aldol reaction between cyclohexanone and benzaldehyde, catalyzed by a family of tag-free and ionic-tagged prolines, are presented. Whereas diastereo- and enantioselectivities remain very high in all cases examined, the ion-tagged catalyst *cis*-4-(2-(3-methyl-imidazol-3-ium-1-yl)acetoxy)-proline bistriflimide, *cis*-**7**, displays a remarkably high activity compared to its tagged *trans* analogue and to the tag-free catalysts *cis* and *trans*-4-(2-phenylacetoxy)-proline **8**. A computational investigation of ion-tagged and tag-free model systems shows that the transition state involving *cis*-**7** is stabilized by a complex interplay of hydrogen bonds (in particular, those involving the counter ion oxygen atoms and the hydrogen atoms of the ionic tag), π-stacking interactions involving the aldehyde phenyl ring, and similar π interactions between the proline carboxyl group and the imidazole ring. The overall effect of these interactions accounts for the observed enhanced activity.

Introduction

In the 1980s, while entering the field of asymmetric catalysis through his chiral oxazaborolidines,[1] E. J. Corey coined the term "chemzymes" to define small molecules able to mimic enzymes in the promotion of enantioselective transformations.[2] In the chemical community, the term was only seldom reused, for example, to define rational catalyst design,[3] self-assembled catalytically active supramolecular structures,[4] or soluble polymer-tagged catalysts, large enough to be retained behind an ultrafiltration membrane in the chemzyme membrane reactor technology.[5] In organocatalysis,[6] particularly in reactions promoted by α-amino acids and their derivatives, the term chemzyme fits well with the original meaning, particularly if the relationship between the organocatalytic mechanism and the enzyme process is straightforward. For example, the rate-determining steps in catalytic cycles of proline-catalyzed aldol reactions have been demonstrated to correlate well with those characteristic of class I aldolases, which activate substrates through an iminium ion formation step, followed by conversion to an enamine.[7]

The amazing substrate-, site-, and stereo-selectivities characterizing enzymatic catalysis are the result of multiple bonds of the substrate to the active site through hydrogen bonds, hydrophobic, van der Waals, π-stacking, ion–ion and ion–dipole electrostatic interactions, or a combination of all of these to form the enzyme–substrate complex. As this multiple binding is enabled by the presence of catalytic residues that take part in the chemical reaction, the analysis of these residues in enzyme active sites allows for the rationalization of the enzymatic mechanism.[8] To facilitate this work, the Catalytic Site Atlas, a database documenting enzyme active sites and catalytic residues in enzymes structures, has been developed.[9]

Proline, a prototypical example of organocatalyst, is a bifunctional molecule with 1) a nucleophilic secondary amine devoted to the formation of iminium–enamine species with the donor carbonyl compound and 2) an acidic group that binds the acceptor aldehyde by hydrogen bonding.[10] Over the last 12 years, an outstanding number of research groups have tackled the challenge to improve the original low efficiency of proline by modifying its skeleton. Skeleton modifications are generally accomplished by adding supplementary groups on either the carboxyl or hydroxyl group of *trans* or *cis*-4-hydroxy proline.[11]

With regard to chemzymes, the aim of these structural modifications is to introduce further interactions in the transition state of the rate-limiting addition of enamine to the acceptor aldehyde. For example, extra hydrophobic and van der Waals interactions are expected to be active if **1**,[12] **2**,[13] or **3**[14] are used, whereas proline derivatives **4**,[15] **5**,[16] and **6**[17] offer new hydrogen-bonding opportunities (Figure 1).

[a] *Prof. A. Bottoni, Prof. M. Lombardo, Dr. G. P. Miscione, Dr. E. Montroni, Dr. A. Quintavalla, Prof. C. Trombini*
Dipartimento di Chimica "G. Ciamician"
Università degli Studi di Bologna
via Selmi 2, 40126, Bologna(Italy)
E-mail: marco.lombardo@unibo.it
gianpietro.miscione@unibo.it

[b] *Dr. E. Montroni*
Consorzio Interuniversitario "C.I.N.M.P.I.S."
via Orabona 4, 70125 Bari(Italy)

Supporting information for this article is available on the WWW under http://dx.doi.org/10.1002/cctc.201300399.

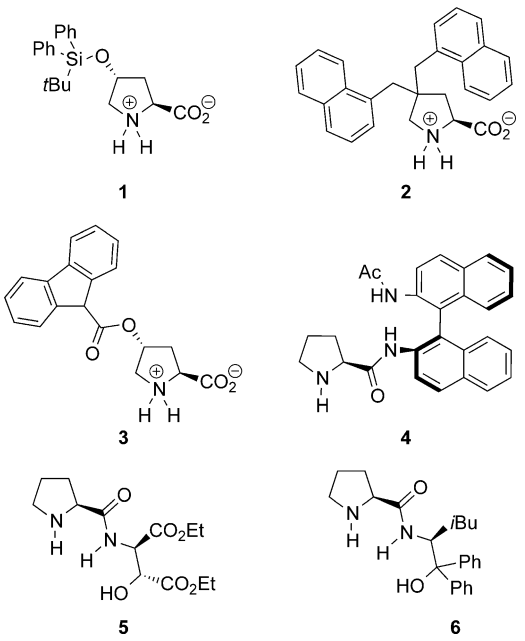

Figure 1. Examples of proline derivatives used as aldolization catalysts. Ac = acetyl.

The synthetic strategy described here is aimed to improve the catalytic performance of proline and implies the insertion of an ionic group onto the original catalyst (proline) to exploit supplementary electrostatic interactions. A schematic representation of a thus designed catalyst is given in Figure 2.

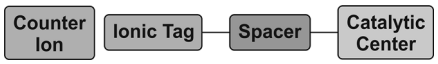

Figure 2. The elementary components of an ion-tagged catalyst.

Our working hypothesis that could explain the observed catalytic effect is based upon the assumption that, if the tagging ion pair can approach charges developing along the reaction coordinate with minimal distortion of bond angles and distances, the final result could be a lowering of the activation barrier by complementing charge separation in the dipolar transition state.[18]

The electrostatic stabilization of a transition state by an ion tag, as examined in the present paper, could be considered a simplified version of the electrostatic activation of enzymatic reactions, which is believed to owe to protein cationic and anionic residues oriented towards the charges of a dipolar transition state.[19] Of course, the presence of the ion pair also determines new steric interactions. As the overall effect is a combination of electrostatic and steric interactions, we defined it as either "electrosteric stabilization" of the transition state by the ion tag or "electrosteric activation" of the catalytic process. Importantly, the ion tag can also affect the stereochemical outcome of the reaction. If parallel reaction pathways leading to stereoisomeric products are accessible, it is conceivable that electrosteric interactions can influence competitive transition states to a different extent, thus favoring the formation of one stereoisomer over the others.

It is interesting to outline that, for the purpose of introducing effective stabilizing effects on transition states, tagging a catalyst with an ionic group requires consideration of the following structural features: 1) the connection point of the spacer, 2) the nature of the ionic group bound covalently to the spacer, 3) the potentially exchangeable counter ion, and 4) the length and flexibility of the spacer, which must ensure the best charge approach with minimal strain energy. All of these aspects were considered in recent studies performed in our lab on ion-tagged proline and prolinol derivatives and, in all cases, appreciable to remarkable increases of reaction rates compared to those of the parent catalysts were recorded.[20] Similar ion-tagged 4-hydroxyproline-derived organocatalysts have also been independently developed by other research groups.[21] Use of an imidazolium ion as the tag was generally investigated first, owing to its well-known capability to favor supramolecular organization by electrostatic, hydrogen-bonding, and/or aromatic-stacking interactions, thus possibly simulating the role of catalytic residues in enzyme catalysis through the promotion of supplementary interactions between reacting species and the cationic receptor in the transition state.[22]

Following on from this, we tried here to assess the entity of the electrosteric effect of an ion tag by a comparative experimental study of the reaction described in Scheme 1. This reaction was promoted, under the same conditions, by 1) two diastereomeric ion-tagged prolines, *trans*-**7** and *cis*-**7** or by 2) the corresponding phenylacetic acid esters *trans*-**8** and *cis*-**8**, isoster analogues of the *N*-methylimidazolium-tagged **7**.

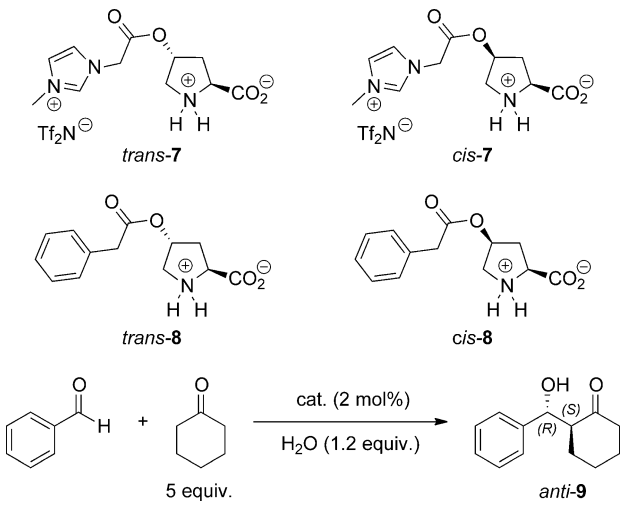

Scheme 1. The benchmark reaction used for the experimental and theoretical comparison of catalysts **7** and **8**. Tf = Trifluoromethanesulfonyl.

In addition to electrostatic and steric interactions, given the nature of the ion tag and the counter ion shown in Scheme 1, other interactions were expected to play important roles in stabilizing the transition state. In particular, hydrogen bonds and π-stacking-like interactions required careful consideration and analysis.

To understand in detail the origin of the catalytic effect and stereochemical outcome, in addition to the experimental study, we performed a computational DFT investigation on the reaction in Scheme 1 that focused on the rate-limiting step, that is, the addition of the resulting enamine to the acceptor aldehyde. To this purpose, we considered two different model systems: model 1 (**m1**) and model 2 (**m2**), which emulated the ion-tagged (*trans*-**7** and *cis*-**7**) and the untagged (*trans*-**8** and *cis*-**8**) systems, respectively.

Results and Discussion

Comparative experimental assessment of the reaction profile with catalysts 7 and 8

The reaction conditions for the selected benchmark reaction (see Scheme 1) were identified in the solvent-free protocol developed previously for **7**,[20b,d] in which a 5-molar excess of cyclohexanone was used to ensure homogeneity in the presence of an almost stoichiometric amount of water. The role of water in organocatalyzed aldol reactions was discussed recently by Gruttadauria and co-workers[23] and rationalized by Armstrong and Blackmond.[24]

To better evaluate reactivity differences, we decided to use the four catalysts *cis*/*trans*-**7** and *cis*/*trans*-**8** at 2 mol% with a moderately reactive aldehyde such as benzaldehyde. Under these conditions with catalyst *cis*-**7**, we obtained a yield of 86% over 19 h, with *ee* > 99% and a 92:8 diastereomeric ratio, favoring the formation of (*S*)-2-[(*R*)-hydroxy-(phenyl)methyl]cyclohexanone (*anti*-**9**, Scheme 1).

The reaction course was checked in each case by taking samples at different time intervals (30 min and 1, 2, 3, 4, 7, and 8 h) and analyzing them by reversed-phase HPLC. Conversions were calculated based on the ratio of *anti*-**9** and benzaldehyde peak areas, having previously determined their corresponding response factors by calibration curves on purified samples. The obtained results are reported in Figure 3.

Inspection of Figure 3 clearly shows that catalyst *cis*-**7** has a far superior activity to both its tagged analogue *trans*-**7** and the untagged catalysts **8**. In all cases examined here, enantioselectivities were almost complete (*ee* > 99%) and diastereomeric ratios were in the 90:10–95:5 range in favor of the *anti*-**9** compound.

Computational results

In this section, we discuss in details the potential energy surface obtained for **m1** and **m2**. As far as we know for these systems (including an imidazolium-tagged proline and its bistriflimide counter ion), computational investigations of comparable accuracy are not available in literature and in the last decade only a few theoretical and kinetic studies have been performed on a very simple model system including only a proline molecule.[25]

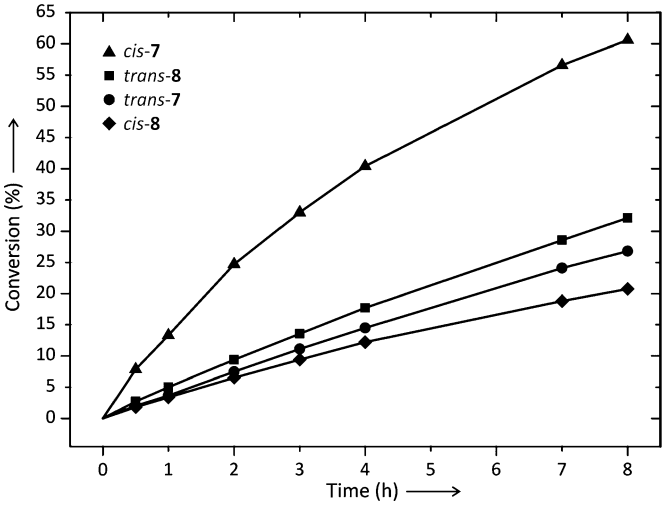

Figure 3. Relative activities of catalysts **7** and **8** in the asymmetric aldol reaction.

m1: A model system including the ionic tag

We discuss first the results obtained for **m1**. In this model, the starting reactants are the enamine molecule (bearing a positive charge formally located on the imidazolium ring) interacting with the bistriflimide counter ion NTf_2^- (**7**, Scheme 1) and a benzaldehyde molecule at infinite distance.

The enamine molecule can exist in different isomeric forms (see Figure 4) depending on two structural features: 1) the *cis* or *trans* configuration of the proline ring (the chain bearing the ionic tag and the proline carboxyl group can be *cis* or *trans*) and 2) the relative position of the carboxyl group and the C=C double bond of cyclohexene, which can be on the same (*syn*) or opposite side (*anti*) relative to the rotation around the N1–C2 bond. Notation regarding the *cis*/*trans* (C/T) configuration relates to substituents at the proline ring system, and the *syn*/*anti* (S/A) enamine conformation is relative to the carboxylic group. For example, **m0**-SC indicates that the C=C double bond and the carboxyl group are on the same side and the proline ring has a *cis* configuration.

Concerning the schematic representation of the four possible isomers of enamine interacting with NTf_2^- reported in Figure 4, the 2D representation makes several atomic distances appear unrealistic and much longer (or shorter) than in the real molecules. Within the carbon framework we have indicated only the hydrogen atoms needed to identify the important hydrogen interactions. The labels used to recognize the various atoms are fortuitous and only a convenient way to identify the atomic centers explicitly referred to in the following discussion. A more realistic 3D picture of all critical points located on the potential surface for **m1** and **m2** is provided in the Supporting Information.

The energies of the four possible reactant isomers (**m0**-SC, **m0**-AC, **m0**-ST, and **m0**-AT) are reported in Figure 5. **m0**-SC and **m0**-AC (a pair of conformational isomers) are quite close in energy (energy difference = 0.8 kcal mol^{-1}), whereas a larger energy gap (3.9 kcal mol^{-1}) is present between the second pair of conformational isomers **m0**-ST and **m0**-AT. Furthermore, the

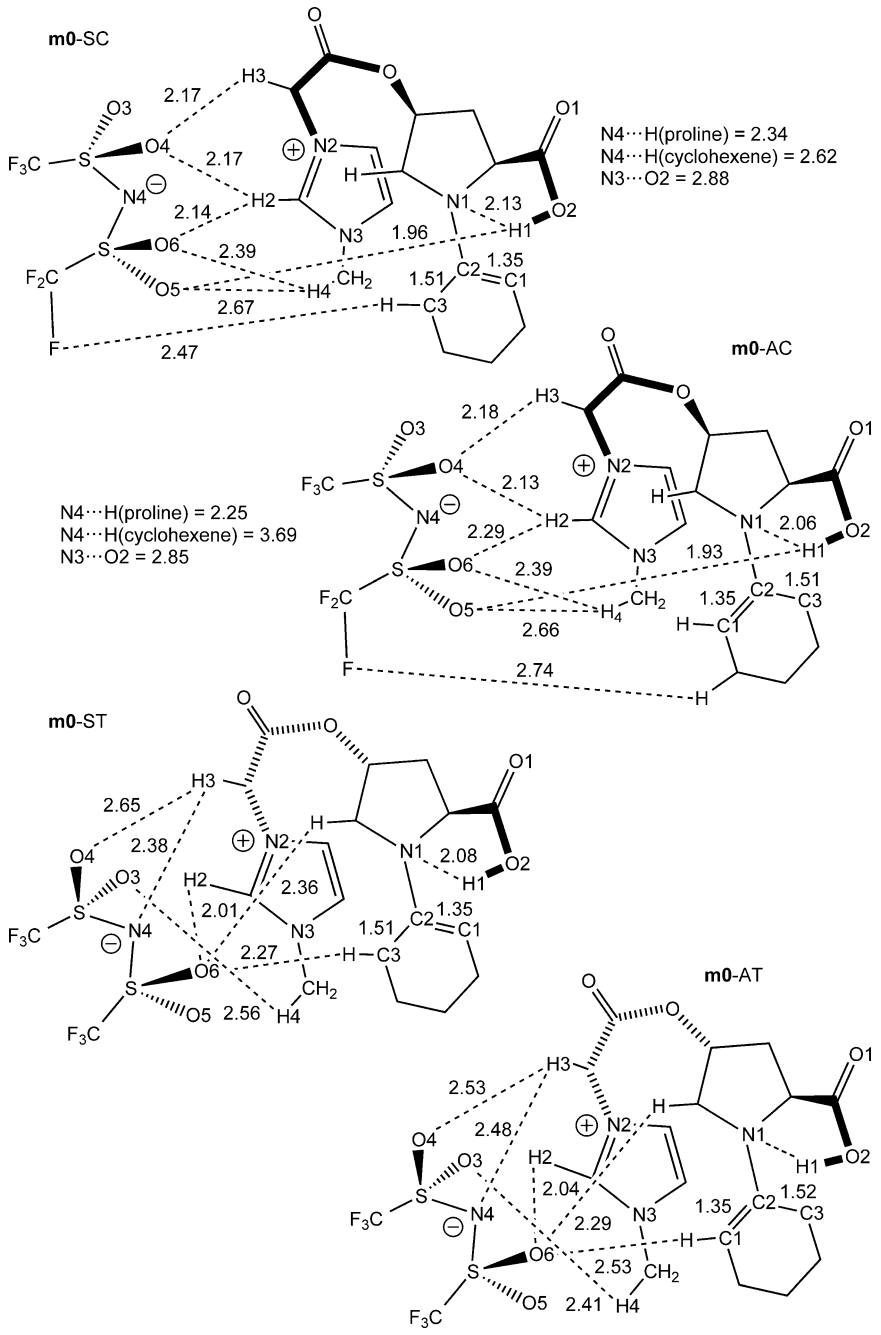

Figure 4. A schematic 2D representation of the various isomers of the enamine molecule interacting with the bistriflimide counter ion NTf_2^- (bond lengths in Å)

trans species are significantly less stable than the *cis* ones, with an energy difference between **m0**-SC (the most stable isomer) and **m0**-ST of 14.0 kcal mol^{-1}.

The calculations on the four isomers show that strong negative charges are localized on the fluorine and oxygen atoms of the bistriflimide anion. As a consequence, these atoms form a complex network of hydrogen bonds that involves the hydrogen atoms on the positive imidazole ring, those of the side chain bearing imidazole, the cyclohexene moiety, and the proline carboxyl group. This network (evidenced in Figure 4) is almost identical compared to the two most stable species **m0**-SC and **m0**-AC. The strongest interaction is between one bistriflimide oxygen (O5) and the acidic hydrogen atom (H1) of the carboxylic group (the O5···H1 distance is 1.96 and 1.93 Å in **m0**-SC and **m0**-AC, respectively). Three additional strong interactions involve O4 and O6, one methylene hydrogen atom H3 and the most acidic imidazole hydrogen atom H2 (0.43 is the net positive charge on this hydrogen atom in **m0**-SC): these interactions are almost identical across the two species. A further interaction involves a bistriflimide fluorine atom and a hydrogen atom on the cyclohexene ring. This interaction varies significantly between **m0**-SC (F···H = 2.47 Å) and **m0**-AC (F···H = 2.74 Å). Furthermore, the bistriflimide negative N4 nitrogen atom (charge −0.86 in **m0**-SC) interacts with the proline hydrogen atom and the cyclohexene hydrogen atom (both evidenced in Figure 4). Although the former interaction remains significant in both species, the latter becomes negligible in **m0**-AC (N4···H(cyclohexene) distance is 2.62 and 3.69 Å, respectively). The regularity of the various hydrogen-bond interactions (with the only exception of the F···H and N4···H(cyclohexene) interactions) can explain the near degeneracy of the two *cis* isomers.

An additional structural feature of both **m0**-SC and **m0**-AC is the folded structure attained by the ionic tag, the spacer and the proline carboxyl group: this particular arrangement brings the imidazolium ring and the proline carboxylic group closer and activates stabilizing π-stacking-like interactions between them. The importance of these interactions should be approximately the same in **m0**-SC and **m0**-AC, as suggested by the N3···O2 distances (2.88 and 2.85 Å, respectively).

The two *trans* isomers show a similar network of hydrogen bonds involving the O3, O4, and O6 oxygen atoms of bistriflimide. However, these interactions are on average less strong than the corresponding interactions in the two *cis* species, as

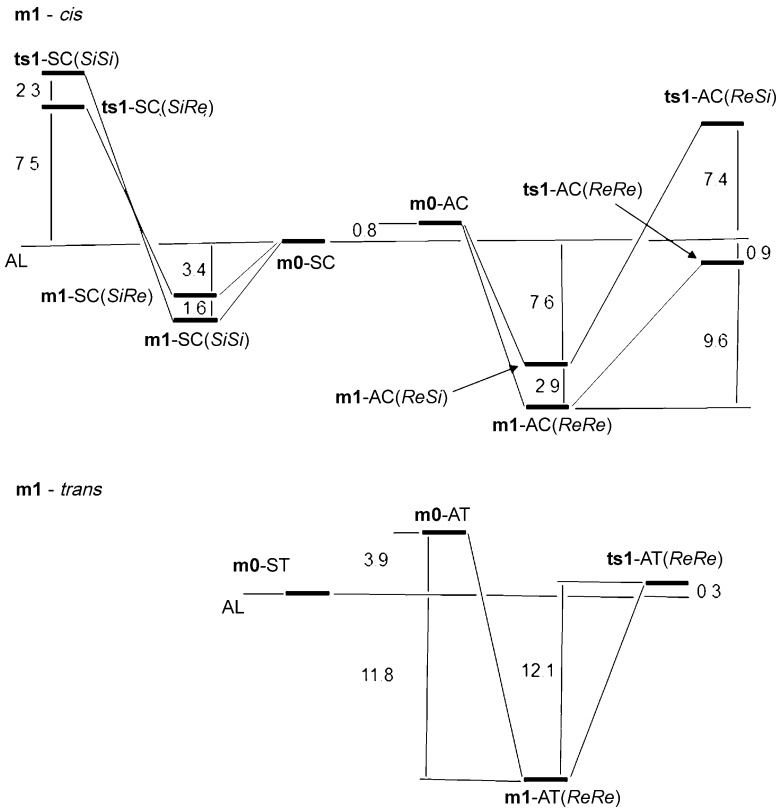

Figure 5. Energies of the *cis* (top) and *trans* (bottom) starting adducts **m0**, the corresponding preliminary intermediates **m1**, and transition states **ts1** obtained for **m1**. Energy values [kcal mol^{-1}] are relative to **m0**-SC and **m0**-ST.

indicated by the longer O···H distances. Furthermore, because of the relative positions of the various molecular fragments (owing to the *trans* configuration of the proline cycle), the important interaction involving O5 and the acidic carboxyl hydrogen atom H1 is now lacking. In addition, the *trans* arrangement of the ionic tag and proline carboxyl group does not allow the stabilizing π-stacking interactions between the carboxyl group and the imidazole ring that are found in the *cis* species. These two factors (i.e., lack of the strong O5···H1 interaction and unfeasibility of the π-stacking interactions) can explain the destabilization of the *trans* isomers.

The aldehyde, if added to the reaction mixture, immediately forms a preliminary complex (**m1**) without overcoming any activation barrier. This complex precedes the transition state for the formation of the new carbon–carbon bond (C1–C4). Depending on which face of aldehyde and enamine (*Re* or *Si* with respect to C4 and C1, respectively) is involved and the structure (*syn* or *anti*) of enamine, in principle eight different approaches are possible for both the *cis* and *trans* isomer.[10c] However, the reaction can proceed only if a hydrogen bond can be established between the aldehyde carbonyl oxygen and the proline carboxylic proton. This hydrogen bond is essential to allow the subsequent hydrogen atom transfer in the reaction. This structural constraint limits the possible orientations of enamine to *anti-Re* and *syn-Si*. For each orientation, either the *Re* or *Si* aldehyde face can be involved, therefore, four possible preliminary complexes **m1** must be considered.

The energy positions of these **m1** complexes with respect to the bistriflimide–enamine complex and benzaldehyde at infinite distance (reactants) are shown in Figure 5. In these diagrams, two different reference reactant energies [or asymptotic limits (ALs)] are used: one for the *cis* species (**m0**-SC) and one for the *trans* species (**m0**-ST), both reported in the center of the diagram. To label the various complexes, we have chosen new names that collect information on the structure of the enamine and the faces of enamine and aldehyde involved in the attack. For example, **m1**-AC(*ReSi*) denotes a complex that originates from the *anti–cis* enamine (i.e., **m0**-AC) and in which the *Re* face of enamine and the *Si* face of the aldehyde are reacting. It is apparent from Figure 5 that, starting from the two *cis* enamine isomers and the aldehyde at infinite distance, the formation of the preliminary complex leads in all cases to a significant stabilization of the system, which is stronger for the two complexes originating from **m0**-AC, that is, **m1**-AC(*ReSi*) and **m1**-AC(*ReRe*): 7.6 and 10.5 kcal mol^{-1} lower than AL, respectively. A significant, even less pronounced stabilization, features in the formation of **m1**-SC(*SiSi*) and **m1**-SC(*SiRe*): 5.0 and 3.4 kcal mol^{-1} below AL, respectively. A similar behavior is found for the **m1** complex that originates from **m0**-AT, that is, **m1**-AT(*ReRe*), which is 11.8 kcal mol^{-1} below AL.

Also in Figure 5, we report the energy of the transition states (**ts1**) that follow the preliminary complexes **m1**. The resulting four reaction channels (starting from the two *cis* isomers) shown can explain the observed diastereoselectivity. In the first phase of the reaction, the system equilibrates to form the most stable preliminary complex **m1**-AC(*ReRe*), which becomes highly dominant (we must remember that a conformational equilibrium connects **m0**-SC and **m0**-AC). Furthermore, as **ts1**-AC(*ReRe*) is the lowest energy transition state (0.9 kcal mol^{-1} below AL) the reaction proceeds along the **m1**-AC(*ReRe*)→**ts1**-AC(*ReRe*) reaction path affording product *anti*-**9**, which is characterized by *R* and *S* configurations at the new chiral centers, as indicated in Scheme 1. This kinetic behavior could relate to the Curtin–Hammett principle: the four complexes of **m1** can be considered interconverting conformational isomers and the preferred path is determined by the relative energy of the four corresponding transition states of **ts1**.

Analysis of the structural features of the four complexes **m1** reported in Figure 6 can help to justify their relative energies

and the major stability of **m1**-AC(*ReRe*). In all four species, the benzaldehyde molecule inserts itself into the hole formed by the proline on one side and the ionic tag and counter ion NTf_2^- on the other side. This approach does not significantly alter most of the hydrogen bond network found in the starting complexes. The most significant variation in the network is the disappearance of the strong O5···H1 interaction, which is made unattainable by the aldehyde insertion and is replaced by a similarly strong interaction between the aldehyde oxygen O7 and the acidic hydrogen atom H1 (the O7···H1 distance is 1.74 Å in **m1**-AC(*ReRe*)).

However, the most interesting feature, which differentiates the **m1**-AC and the **m1**-SC pairs is the special position adopted by the aldehyde benzene ring in the former case. In both **m1**-AC(*ReRe*) and **m1**-AC(*ReSi*) complexes, the benzene moiety faces the NTf_2^- oxygen atoms (O3 in the former and O5 and O6 in the latter), an arrangement that activates stabilizing π-stacking-like interactions between the π oxygen lone pairs and the benzene π electron cloud. Typical distances between the oxygen atoms and the most effectively interacting benzene carbon atoms are in the range 3.0–3.3 Å, as reported in Figure 6. In the **m1**-SC pair, obtained after rotation of the cyclohexene ring around the N1–C2 bond, the aldehyde is too far away from NTf_2^- and these π interactions disappear.

A further stabilization of both **m1**-AC(*ReRe*) and **m1**-AC(*ReSi*) owes to π-stacking interactions between the imidazole ring and the proline carboxyl group. These interactions, which are similar to those detected in the starting complexes, are absent in the **m1**-SC pair, in which the aldehyde insertion does not allow the system to achieve the necessary folded arrangement of the ionic tag, spacer, and proline carboxyl group. The above-discussed structural features reasonably explain the lower energies of the two **m1**-AC intermediates compared to those of **m1**-SC. Furthermore, the lower energy of **m1**-AC(*ReRe*) compared to **m1**-AC(*ReSi*) is mainly a consequence of the larger steric interactions between the benzene ring and the enamine cyclohexene ring observed in the latter case. This causes a weakening of the O7···H1 hydrogen bond (the O7···H1 distance is 1.74 and 1.89 Å in the two intermediates) and a larger C1···C4 distance (the incipient bond), which is 3.13 and 3.95 Å in **m1**-AC(*ReRe*) and **m1**-AC(*ReSi*), respectively. Also, the replacement of the O5···H5 hydrogen bond (O5···H5 distance = 2.38 Å)

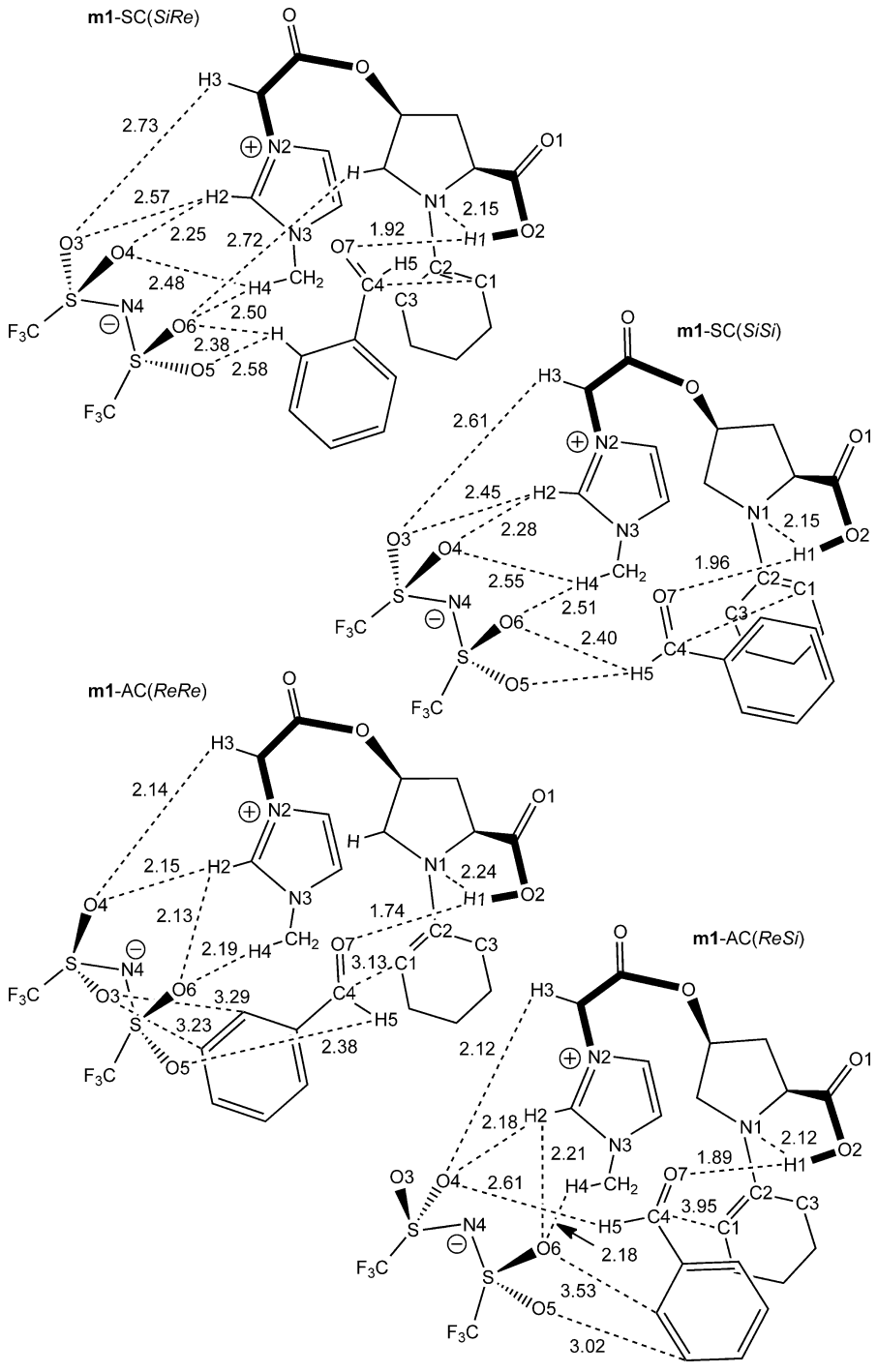

Figure 6. A schematic 2D representation of the preliminary complexes **m1**-SC(*SiRe*), **m1**-SC(*SiSi*), **m1**-AC(*ReRe*) and **m1**-AC(*ReSi*) (bond lengths in [Å]).

by the weaker O4···H5 interaction (O4···H5 distance = 2.61 Å) on passing from **m1**-AC(*ReRe*) to **m1**-AC(*ReSi*) certainly increases the stability of the former species compared to the latter. It is likewise important to examine the structural features of the transition states **ts1** (in particular **ts1**-AC(*ReRe*) and **ts1**-AC(*ReSi*), depicted in Figure 7) and how these features determine their relative energies and the kinetics of the process.

ts1 Describes the formation of the new C1···C4 bond and the simultaneous hydrogen atom transfer from O2 to O7. In the lowest energy transition state **ts1**-AC(*ReRe*), the C1···C4 distance between the two approaching carbon atoms C1 and C4 is 2.20 Å and the O7···H1 and H1···O2 distances are 1.17 and 1.23 Å, respectively. This transition structure closely resembles the preceding intermediate **m1**. The two structures show a very similar pattern of hydrogen bonds involving the NTf_2^- oxygen atoms and the hydrogen atoms of the ionic tag. Furthermore, π-stacking-like interactions between the NTf_2^- oxygen lone pairs and the aldehyde benzene ring and between the proline carboxyl group and the imidazole ring can be envisaged: in the former, the distances between O3 and the closest benzene carbon atoms are 3.31 and 3.22 Å, whereas in the latter, the distances between O2 and N3 and between O1 and the imidazole carbon adjacent to N3 are 2.87 and 3.27 Å, respectively. Interestingly, the N1···H1 hydrogen bond evidenced in **m1**-AC(*ReRe*) (N1···H1 distance = 2.24 Å) is maintained in the transition state, in which this distance is 2.43 Å. Thus, the proline nitrogen can be thought to behave like a proton shuttle that "assists" the hydrogen atom transfer by stabilizing the transition state. In addition to this "assistance", the above-described π-stacking interactions certainly contribute to stabilize the transition state and facilitate the proton transfer. Finally, a further important hydrogen bond involves O5 and the aldehyde hydrogen atom H5 (H5···O5 distance = 2.22 Å).

The structure of **ts1**-AC(*ReSi*) is similar to that of **ts1**-AC(*ReRe*). However, two interesting differences must be pointed out: the disappearance of the H5···O5 interaction that is replaced by the weaker H5···O4 interaction (H5···O4 distance = 2.56 Å in **ts1**-AC(*ReSi*); H5···O5 distance = 2.22 Å in **ts1**-AC(*ReRe*)) and the simultaneous weakening of the π-stacking interactions between the proline carboxyl group and imidazole. The weakening of these interactions is caused by a change in the orientation of the proline carboxyl group that determines the increase in the distance between O1 and the closest imidazole carbon atom (3.41 Å). Furthermore, the different aldehyde orientation causes a larger steric interaction between the benzene ring and the enamine cyclohexene ring, similar to that detected in the previous intermediate. These structural differences can reasonably explain the higher energy of **ts1**-AC(*ReSi*) compared to **ts1**-AC(*ReRe*).

Also, we have considered the **m1** intermediate originating from the **m0**-AT starting complex and involving the two *Re* faces in the formation of the new C1–C4 bond. This intermediate, denoted as **m1**-AT(*ReRe*) is 11.8 kcal mol^{-1} below the corresponding asymptotic limit and identifies the reaction channel leading to the observed final product with *R* configuration at the new chiral center. Schematic representations of **m1**-AT(*ReRe*) and the following transition state **ts1**-AT(*ReRe*) are given in Figure 8.

It is important to compare the intrinsic activation energy of the two reaction channels **m1**-AT(*ReRe*)→**ts1**-AT(*ReRe*) and **m1**-AC(*ReRe*)→**ts1**-AC(*ReRe*): these are 12.1 and 9.6 kcal mol^{-1}, respectively. These values clearly indicate that the former process is significantly slower than the latter in agreement with the experimental evidence.

The observed increase of activation energy can be explained by comparing the two structures **m1**-AT(*ReRe*) and **ts1**-AT(*ReRe*) and recalling the previous discussion on **m1**-AC(*ReRe*) and **ts1**-AC(*ReRe*). In **m1**-AT(*ReRe*) we can recognize the usual hydrogen bonds involving the NTf_2^- oxygen atoms (mainly O4 and O6), the H2 imidazole hydrogen atom, and the H4 hydrogen atom on the imidazole methyl group (O6···H2 interaction is important, the distance being2.10 Å). In addition, O5 in-

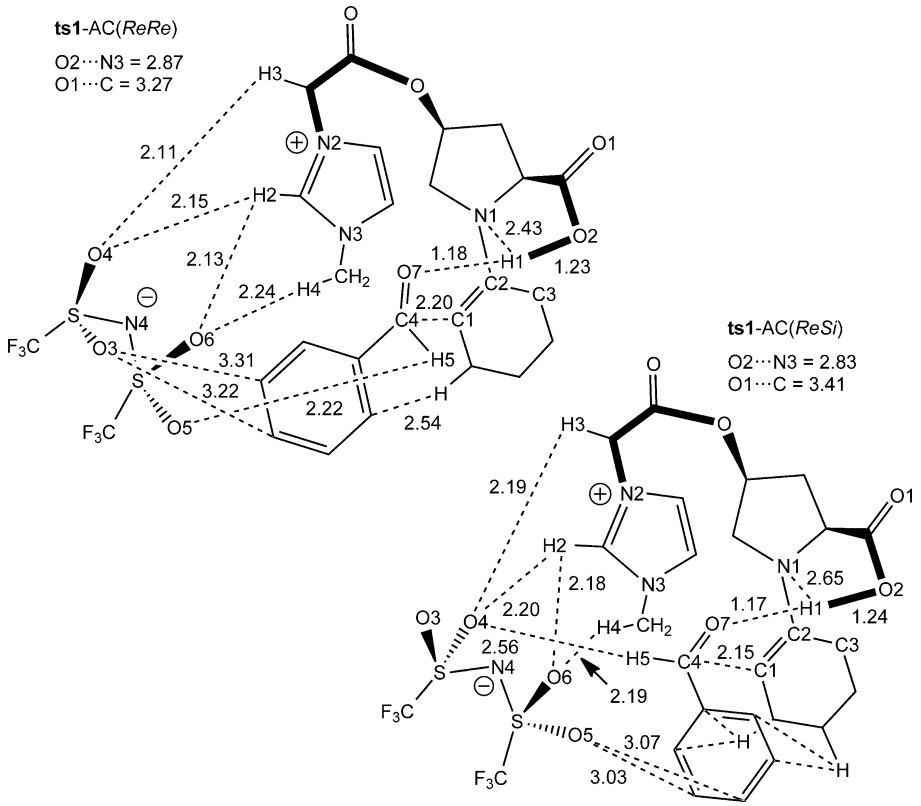

Figure 7. A schematic 2D representation of the transition states **ts1**-AC(*ReRe*) and **ts1**-AC(*ReSi*) (bond lengths in [Å]).

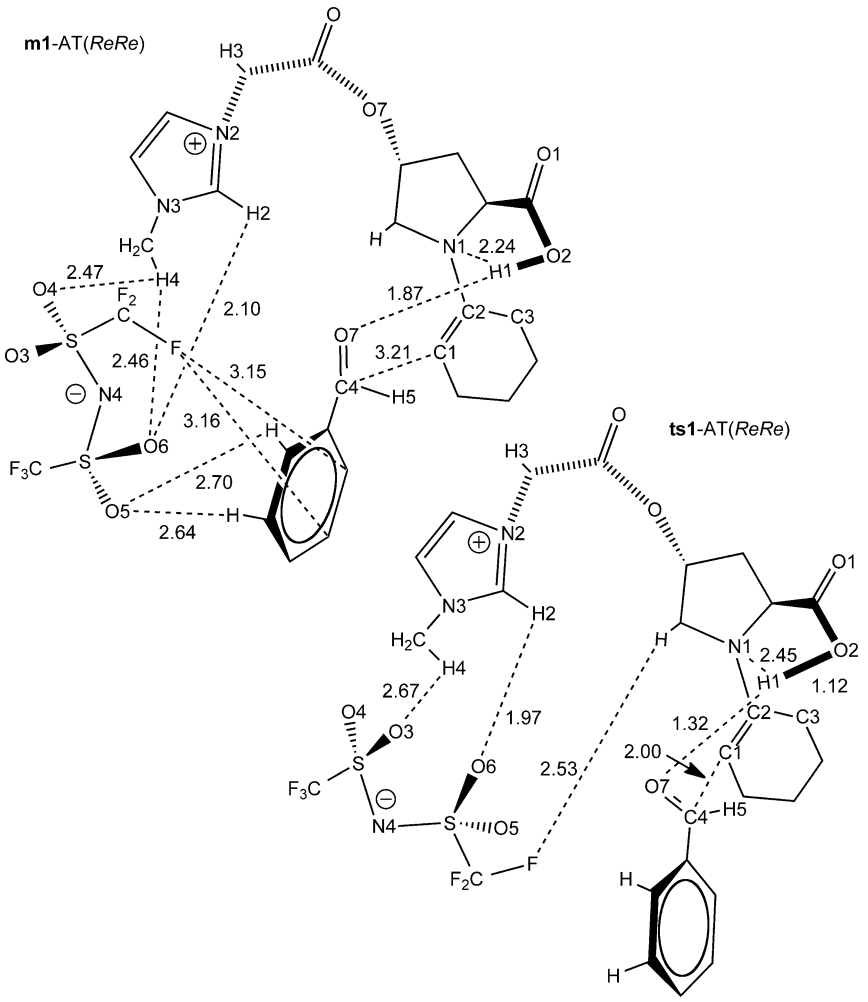

Figure 8. A schematic 2D representation of the preliminary complex **m1**-AT(*ReRe*) and the following transition state **ts1**-AT(*ReRe*) (bond lengths in [Å]).

teracts with two hydrogen atoms on the benzaldehyde ring and one fluorine atom of to NTf_2^- interacts with the π electron cloud of the same benzene ring (π-stacking-like interactions): the distances between fluorine and the closest benzene carbon atoms are 3.15 and 3.16 Å, as expected for this class of interactions.[26,27] As noted previously, a strong hydrogen bond involves the aldehyde oxygen O7 and the acidic hydrogen atom H1 and anticipates the hydrogen atom transfer occurring in the next transition state. In **ts1**-AT(*ReRe*), to form the new C4–C1 bond and facilitate the hydrogen atom transfer from O2 to O7 by maintaining the H1···O7 interaction, the aldehyde moves away from NTf_2^-, thus causing the disappearing of the above-mentioned stabilizing π-stacking interactions. This molecular rearrangement occurring along the **m1**-AT(*ReRe*)→**ts1**-AT(*ReRe*) reaction path is different to observations along the previously described *cis* channel **m1**-AC(*ReRe*)→**ts1**-AC(*ReRe*) in which the various stabilizing π-stacking interactions (in particular those involving the phenyl ring) are maintained. This evidence provides a reasonable explanation of the larger activation barrier found along the *trans* channel.

m2: A model system in which a phenyl group replaces the ionic tag

To evaluate in detail the effect of the ionic tag on the reaction profile (stereochemical output and efficiency), we discuss here the results obtained for **m2** (untagged system) in which a phenyl ring replaces the positively charged imidazole, but the same side chain O(C=O)CH_2 (spacer) connects the phenyl ring to proline (**8** in Scheme 1). The starting reactants are the enamine molecule bearing the phenyl ring and a benzaldehyde molecule at infinite distance.

In line with the previous discussion, the four possible isomers of the starting untagged enamine are denoted as **m2**-SC, **m2**-AC, **m2**-ST, and **m2**-AT. The corresponding energies are reported in Figure 9 (these asymptotic energies include the energy of a benzaldehyde molecule at infinite distance). The two *cis* conformational isomers **m2**-SC and **m2**-AC are almost degenerate (the former is only 0.6 kcal mol^{-1} more stable than the latter). There is a less negligible energy difference (1.5 kcal mol^{-1}) between the *trans* conformational isomers **m2**-ST and **m2**-AT.

The kinetic scheme featuring the untagged system is similar to that discussed in the previous section for the ionic model: preliminary complexes (**m3**) between the aldehyde and enamine are formed, followed by transition states (**ts2**) for the formation of the new C1–C4 bond and the simultaneous hydrogen atom transfer from O2 to the aldehyde oxygen O3. Within this scheme, the Curtin–Hammet principle can be again invoked (Figure 9).

For both the *cis* and *trans* isomer, we have reported the transition states corresponding to the four possible reaction channels that can be envisaged if we consider the aldehyde face (*Re* or *Si*) and the enamine structure (*syn* or *anti*) involved in the reaction. Interestingly, the lowest energy transition state of the *cis* species, which determines the favored reaction path, is **ts2**-AC(*ReRe*), leading to the formation of the experimentally observed product (*anti*-**9**, Scheme 1). Similarly, for the *trans* species, the lowest energy transition state is **ts2**-AT(*ReRe*), affording *anti*-**9**. Thus, the stereochemical prediction is again in agreement with the experimental evidence.

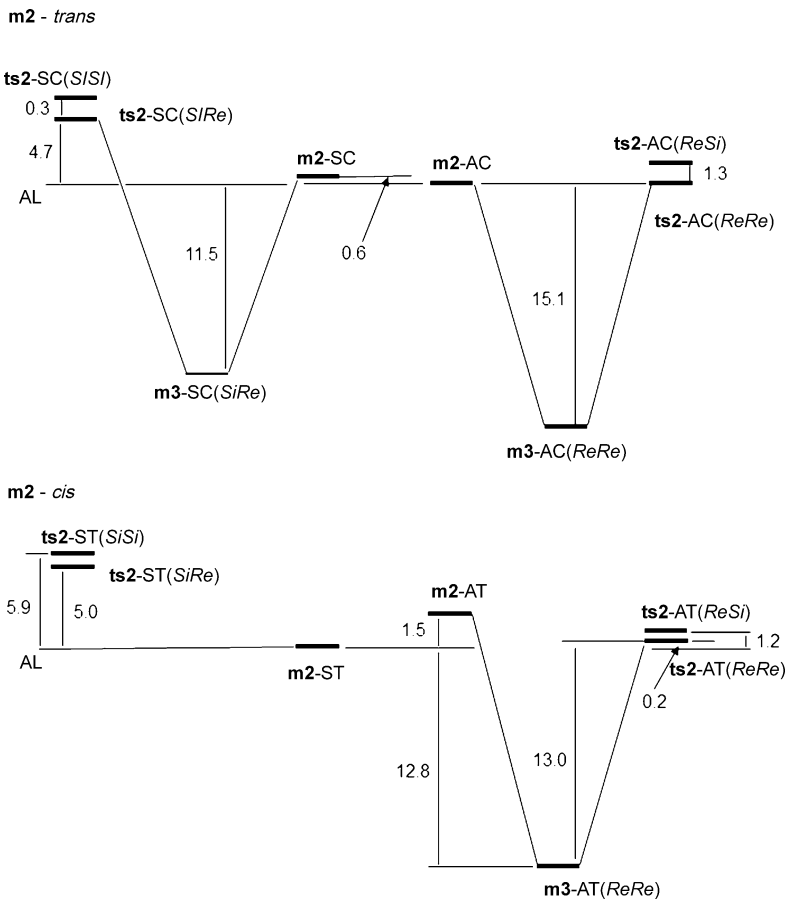

Figure 9. Energies of the *cis* (top) and *trans* (bottom) starting adducts **m2**, the corresponding preliminary intermediates **m3**, and transition states **ts2** obtained for **m2**. Energy values [kcal mol^{-1}] are relative to **m2**-AC and **m2**-ST.

Notably, the intrinsic activation barriers for **ts2**-AC(*ReRe*) and **ts2**-AT(*ReRe*) (15.1 and 13.0 kcal mol^{-1}, respectively) are both significantly larger than the barrier computed for **ts1**-AC(*ReRe*) (9.6 kcal mol^{-1}). This clearly indicates the higher efficiency of the latter process and the catalytic effect of the ionic tag, as experimentally observed. In Figure 10, we schematically depict the two preliminary complexes **m3**-AC(*ReRe*) and **m3**-AT(*ReRe*) and the corresponding transition states **ts2**-AC(*ReRe*) and **ts2**-AT(*ReRe*). The major difference that we have discovered in comparing the transformation **m3**-AC(*ReRe*)→**ts2**-AC(*ReRe*) to the analogous transformation **m1**-AC(*ReRe*)→**ts1**-AC(*ReRe*) within the tagged system is the absence in the former case of a folded enamine structure, that is, the arrangement required to bring the ionic tag (the positively charged imidazolium ring) and the proline carboxyl group closer and to activate stabilizing π-stacking interactions between the two fragments. If a benzene ring is used instead of imidazolium (as in **m2**), these interactions disappear (see **m3**-AC(*ReRe*), Figure 10) and are replaced by interactions between the C–H bond of the aldehyde phenyl ring and the π-electron cloud of the benzene ring bonded to proline in a typical T-shape-like arrangement, as evidenced in Figure 10. Here, the reported values of the two shortest C–H···C(benzene) distances are 2.65 and 2.83 Å. T-shaped C–H···π interactions almost disappear in **ts2**-AC(*ReRe*) (the shortest C–H···C(benzene) distance becomes 3.05 Å), thus explaining the higher activation energy computed for this transition state.

Similar interactions (now involving the benzene bonded to proline and the C–H bonds of the cyclohexene ring) are detected along the **m3**-AT(*ReRe*)→**ts2**-AT(*ReRe*) reaction path. Typical C–H···C(benzene) distances computed for **m3**-AT(*ReRe*) are 2.81 and 2.85 Å (see again Figure 10). However, these interactions remain almost the same in **ts2**-AT(*ReRe*) (C–H···C(benzene) distances become 2.86 and 2.88 Å). Even if these interactions are not as effective as the π-stacking interactions in **m1**, their presence along the **m3**-AT(*ReRe*)→**ts2**-AT(*ReRe*) reaction path contributes to a reduction of the activation barrier from 15.0 to 13.0 kcal mol^{-1}.

Conclusions

In this combined experimental–theoretical study, we have examined the importance of new interactions (π-stacking, hydrogen bonds) that emerge in the rate-limiting aldol transition state owing to the presence of ion-tagged prolines. In particular, we have analyzed in detail the interactions responsible for the superior activity of *cis*-**7** compared to a simple proline, where the above-mentioned interactions were lacking, and compared to its isomer *trans*-**7** and the species *cis*-**8** and *trans*-**8** with similar steric biases but lacking a neat charge on the substituent at C4 of the proline ring system.

The mechanism of the reaction has been investigated by using a computational DFT approach and two model systems, model 1 (**m1**) and model 2 (**m2**) to emulate the ion-tagged (**7**, Scheme 1) and untagged systems (**8**, Scheme 1), respectively.

The results obtained for **m1** can be summarized as follows:

1) Four enamine isomers, all interacting with the bistriflimide counter ion NTf_2^-, exist: two almost degenerate *cis* species (**m0**-SC and **m0**-AC) and two *trans* species (**m0**-ST and **m0**-AT), which are much higher in energy.
2) As the reaction between enamine and benzaldehyde can occur only if a hydrogen bond is activated between the aldehyde carbonyl oxygen and the proline carboxylic proton (this hydrogen bond anticipates the subsequent hydrogen atom transfer that accompanies the new C–C bond formation), only the *Re* face of the *anti* enamine and the *Si* face of the *syn* enamine can react effectively. Furthermore, since

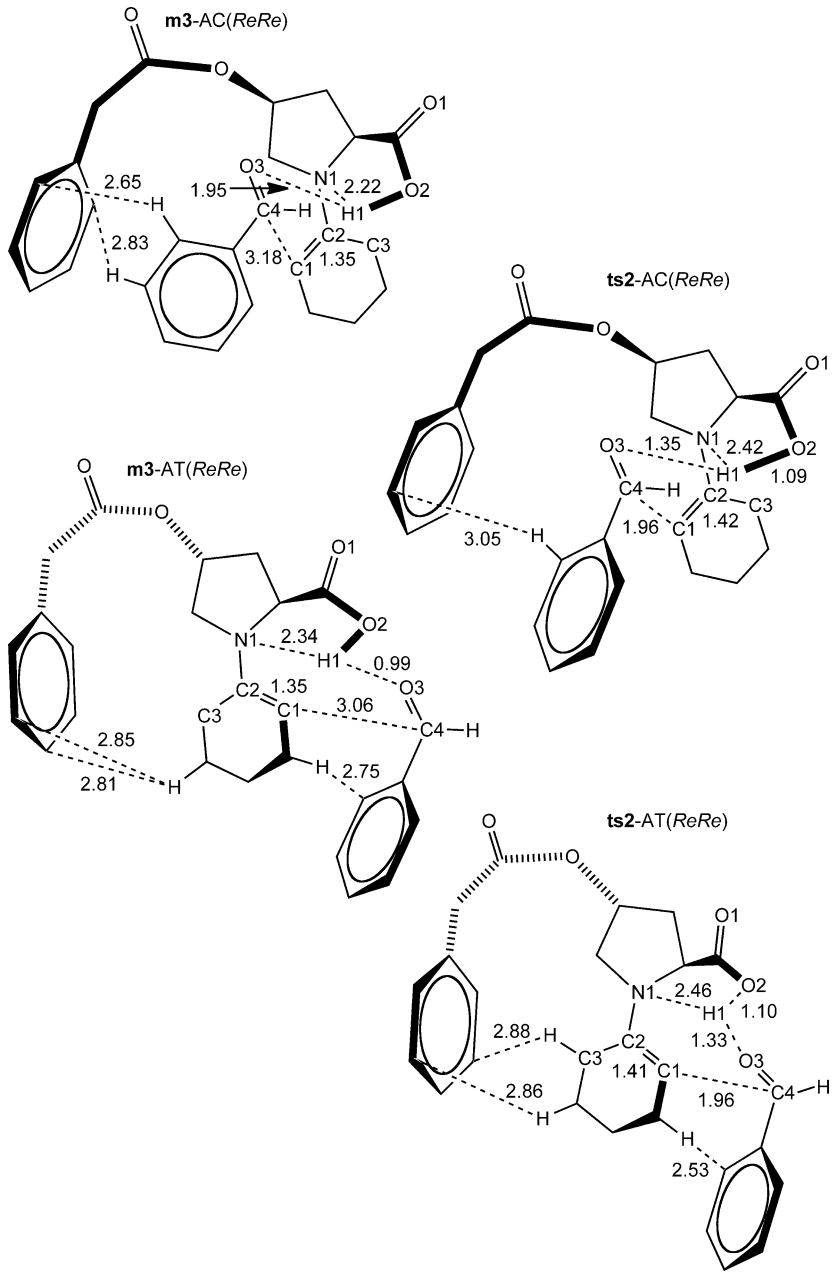

Figure 10. A schematic 2D representation of the preliminary complexes **m3**-AC(*ReRe*) and **m3**-AT(*ReRe*) and the following transition states **ts2**-AC(*ReRe*) and **ts2**-AT(*ReRe*) (bond lengths in [Å]).

either the *Re* or *Si* aldehyde face can be involved, four approaches leading to four different preliminary complexes of **m1** between enamine and aldehyde must be considered. All preliminary complexes are strongly stabilized relative to the reactants.

3) The relative energies of the transition states **ts1** located along the four reaction channels account for the observed stereoselectivities. The lowest energy transition state is **ts1**-AC(*ReRe*), which is structurally similar to complex **m1**-AC(*ReRe*). As a consequence of the Curtin–Hammett principle, the reaction proceeds along the **m1**-AC(*ReRe*)→**ts1**-AC(*ReRe*) reaction path, which affords product *anti*-**9** characterized by *R* and *S* configurations at the newly formed stereogenic centers, in agreement with the experimental results.
4) The structural features of the four **m1** complexes elucidate their relative energy and the major stability of **m1**-AC(*ReRe*). Stabilizing π-stacking-like interactions between the NTf_2^- π oxygen lone pairs and the π electron cloud of benzaldehyde exist possibly only in the **m1**-AC pair and not in the **m1**-SC pair. A further stabilization of both **m1**-AC(*ReRe*) and **m1**-AC(*ReSi*) owes to π-stacking interactions between the imidazole ring and the proline carboxyl group. These interactions are possible only if the system can achieve a suitable folded arrangement of the ionic tag, the spacer, and proline carboxyl group. This occurs in **m1**-AC(*ReRe*) and **m1**-AC(*ReSi*) but not in **m1**-SC(*SiRe*) or **m1**-SC(*SiSi*). Finally, steric interactions between the benzaldehyde phenyl ring and the enamine cyclohexene ring destabilize **m1**-AC(*ReSi*) relative to **m1**-AC(*ReRe*).
5) The strong stabilization of **ts1**-AC(*ReRe*), which closely resembles the preceding intermediate **m1**, is the result of a complex interplay of hydrogen bonds (in particular, those involving the NTf_2^- oxygen atoms and the hydrogen atoms of the ionic tag), π-stacking-like interactions between the NTf_2^- oxygen lone pairs, and the aldehyde phenyl ring, and similar interactions between the proline carboxyl group and the imidazole ring. Furthermore, during the migration the hydrogen atom H1 interacts with the proline nitrogen N1 (N1···H1 distance = 2.43 Å in **ts1**-AC(*ReRe*)), so this nitrogen atom can be thought to behave like a proton shuttle that "assists" the hydrogen atom transfer by stabilizing the corresponding transition state.
6) The activation barriers computed along the *trans* and *cis* reaction channels **m1**-AT(*ReRe*)→**ts1**-AT(*ReRe*) and **m1**-AC(*ReRe*)→**ts1**-AC(*ReRe*) leading to the observed products (12.1 and 9.6 kcal mol^{-1}, respectively) clearly indicate that

the former process must be significantly slower than the latter in agreement with the experimental evidence.

The results obtained for **m2** provide a rationale for the lesser catalytic effect observed experimentally for catalysts **8** and can be summarized as follows:

7) As found for **m1**, the two *cis* conformational isomers **m2**-SC and **m2**-AC are almost degenerate (energy difference = 0.6 kcal mol^{-1}). The energy gap increases to 1.5 kcal mol^{-1} for the *trans* conformational isomers **m2**-ST and **m2**-AT. The topologies of the reaction surfaces are similar to that found for **m1**, that is, preliminary complexes **m3** form, followed by transition states **ts2** (new C–C bond formation and simultaneous hydrogen atom transfer). Within this scheme, the Curtin–Hammet principle can be again invoked.
8) The intrinsic activation barriers for **ts2**-AC(*ReRe*) and **ts2**-AT-(*ReRe*) (15.1 and 13.0 kcal mol^{-1}, respectively) are both significantly larger than the barrier computed for the ion-tagged system along the *cis* pathway, that is, **ts1**-AC(*ReRe*) (9.6 kcal mol^{-1}). This clearly shows the effect of the ionic tag on the reaction rate, as observed experimentally.
9) In the comparison between the tagged and the untagged system, the major difference indicated by our computations is the absence in the latter case of the folded enamine structure found in **m1**, that is, the particular arrangement that brings the ionic tag (a positively charged imidazolium ring) and the proline carboxyl group closer and activates stabilizing π-stacking interactions between the two fragments. If a benzene ring replaces the imidazole group, these interactions disappear. They are replaced by interactions between the C–H bond of the aldehyde phenyl ring and the π electron cloud of the benzene ring bonded to proline. As these interactions are active only in the preliminary complex (**m3**-AC(*ReRe*)) and not in the following transition state (**ts2**-AC(*ReRe*)), the resulting barrier for the untagged system increases significantly.

Cumulatively, points 1–9) represent what we defined in the Introduction as "electrosteric stabilization" of the lowest transition state **ts1**-AC(*ReRe*) by the ionic tag.

Experimental Section

Preparation of catalysts

Catalysts *cis*-**7**, *trans*-**7** and *trans*-**8** were prepared according to literature procedures.[20b,c,28]

cis-**8**: A solution of diethyl azodicarboxylate (DEAD) (0.824 mL, 1.8 mmol) in anhydrous THF (3 mL) was added dropwise to an ice-cold solution of triphenylphosphine (0.432 g, 1.65 mmol), phenylacetic acid (0.215 g, 1.58 mmol), and *N*-benzyloxycarbonyl-(2*S*,4*R*)-4-hydroxyproline benzyl ester (0.533 g, 1.5 mmol) in anhydrous THF (8 mL). The reaction mixture was allowed to warm to RT and stirred for a further 24 h. Concentration of the reaction mixture in vacuo followed by silica-gel column chromatographic purification of the residue (cyclohexane/ethyl acetate 90:10) furnished quantitatively the *cis*-phenyl acetate. $[\alpha]_D^{20} = -39.9$ cm^3 g^{-1} dm^{-1} ($c = 0.90$, $CHCl_3$); ^{1}H NMR (400 MHz, $CDCl_3$, two conformational isomers ≈1:1) $\delta = 2.31$–2.38 (m, 2H), 2.39–2.53 (m, 2H), 3.29–3.41 (m, 4H), 3.58–3.53 (m, 2H), 3.76–3.87 (m, 2H), 4.55 (dd, $J = 2.1$, 9.4 Hz, 1H), 4.64 (dd, $J = 2.2$, 9.3 Hz, 1H), 5.00–5.08 (m, 2H), 5.08–5.13 (m, 2H), 5.13–5.18 (m, 2H), 5.18–5.23 (m, 2H), 5.23–5.30 (m, 2H), 7.15–7.21 (m, 4H), 7.22–7.41 ppm (m, 26H); ^{13}C NMR (100 MHz, $CDCl_3$, two conformational isomers ≈1:1) $\delta = 171.3$, 171.0, 170.97, 170.87, 154.7, 154.3, 136.4, 135.7, 135.6, 133.4, 129.29, 129.27, 128.65, 128.56, 128.51, 128.45, 128.4, 128.21, 128.16, 128.10, 128.04, 127.96, 127.2, 73.2, 72.2, 67.4, 67.3, 67.0, 66.9, 58.1, 57.8, 52.7, 52.4, 40.9, 36.4, 35.4 ppm; elemental analysis calcd for $C_{28}H_{27}NO_6$ (473.52): C, 71.02; H, 5.75; N, 2.96; found: C, 71.69; H, 5.69; N, 2.95.

The intermediate *cis*-phenyl acetate was dissolved in MeOH, 10% palladium on charcoal (0.160 g, 0.15 mmol) was added and the mixture stirred under hydrogen at RT under atmospheric pressure for 24 h. It was then filtered on Celite by washing 5 times with CH_3CN (5 mL). The organic phase was evaporated in vacuo to provide the catalyst *cis*-**8** as a solid (0.334 g, 89% yield). $[\alpha]_D^{20} = -16.4$ cm^3 g^{-1} dm^{-1} ($c = 0.61$, CH_3OH); ^{1}H NMR (400 MHz, CD_3OD) $\delta = 2.43$–2.54 (m, 1H), 2.54–2.64 (m, 1H), 3.43–3.53 (m, 1H), 3.53–3.61 (m, 1H), 3.64 (s, 2H), 4.13 (dd, $J = 3.6$, 9.9 Hz, 1H), 5.27–5.33 (m, 2H), 7.21–7.36 ppm (m, 5H); ^{13}C NMR (100 MHz, CD_3OD) $\delta =$ 172.59, 172.55, 135.1, 130.5, 129.5, 128.1, 74.2, 65.6, 52.0, 41.5, 36.1 ppm; elemental analysis calcd for $C_{13}H_{15}NO_4$ (249.26): C, 62.64; H, 6.07; N, 5.62; found: C, 62.32; H, 6.15; N, 5.57.

Aldol reaction

General procedure: Cyclohexanone (0.52 mL, 5 mmol), water (0.022 mL, 1.2 mmol) and benzaldehyde (0.102 mL, 1 mmol) were added to the appropriate catalyst (0.02 mmol) and the mixture was stirred at RT. The reaction mixture was quenched by charging it directly onto a silica-gel column and the pure aldol was obtained upon elution with cyclohexane/ethyl acetate 8:2. The *ee* values were determined by using chiral HPLC with a CHIRALCEL OJ column (hexane/2-propanol 90:10, flow rate = 0.5 mL min^{-1}, $\lambda =$ 220 nm, $T = 40$ °C); t_R *anti* (major) = 15.57 min, t_R *syn* = 16.50 min, t_R *anti* = 18.81 min, t_R *syn* (major) = 21.03 min.

Determination of reaction conversion

A sample of the reaction mixture (10 μL) was diluted in 3 mL of CH_3CN and 5 μL of the resulting solution was injected on HPLC. The retention time for benzaldehyde was 13.6 min and the retention time for the product *anti*-**9** was 22.9 min. HPLC conditions: Eclipse XDB-C18 5 μm column (4.6 mm × 150 mm) with CH_3CN/H_2O 30:70 as the mobile phase and detection at 210 nm, flow rate = 0.5 mL min^{-1}, $T = 30$ °C.

Computational Methods

All computations reported in the paper were performed with the Gaussian09[29] series of programs. As aryl groups and extended π systems were present on both the aldehyde and the catalyst, a functional capable of describing interactions involving π system was required. It is well-known that this class of interaction (in which medium-range correlation effects are dominant) are not described properly by most popular DFT functionals, for example, B3LYP. However, during the last decade new functionals have been recommended that are capable of treating medium-range correlation effects.[30] Within this family of innovative functionals, we have chosen that recently proposed by Truhlar and Zhao, known as

M06-2X, which has been demonstrated to provide a good estimate of π–π interactions and reaction energetics.[30b] All atoms have been described by the DZVP basis,[31] which is a local spin density-optimized basis set of double-zeta quality including polarization functions. The geometries of the various critical points on the potential surface were optimized fully by using the gradient method available in Gaussian 09 and harmonic vibrational frequencies were computed to evaluate the nature of all critical points.

Acknowledgements

Financial support was provided by Miur-Rome (PRIN 20099PKPHH_004), Fondazione del Monte di Bologna e Ravenna, and COST Action CM0905 "Organocatalysis".

Keywords: aldol reaction · asymmetric catalysis · density functional calculations · electrosteric activation · organocatalysis

[1] E. J. Corey, C. J. Helal, *Angew. Chem.* **1998**, *110*, 2092 – 2118; *Angew. Chem. Int. Ed.* **1998**, *37*, 1986 – 2012.
[2] E. J. Corey, C.-P. Chen, G. A. Reichard, *Tetrahedron Lett.* **1989**, *30*, 5547 – 5550.
[3] a) J. Xiao, F.-X. Xu, Y.-P. Lu, T.-P. Loh, *Org. Lett.* **2010**, *12*, 1220 – 1223; b) H. Sasai, T. Arai, Y. Satow, K. N. Houk, M. Shibasaki, *J. Am. Chem. Soc.* **1995**, *117*, 6194 – 6198.
[4] a) G. Hu, A. K. Gupta, R. H. Huang, M. Mukherjee, W. D. Wulff, *J. Am. Chem. Soc.* **2010**, *132*, 14669 – 14675; b) S. Xue, S. Yu, Y. Deng, W. D. Wulff, *Angew. Chem.* **2001**, *113*, 2331 – 2334; *Angew. Chem. Int. Ed.* **2001**, *40*, 2271 – 2274; c) J. Bjerre, C. Rousseau, L. Marinescu, M. Bols, *Appl. Microbiol. Biotechnol.* **2008**, *81*, 1 – 11; d) Y. Zhang, Z. Lu, A. Desai, W. D. Wulff, *Org. Lett.* **2008**, *10*, 5429 – 5432.
[5] J. Wöltinger, A. S. Bommarius, K. Drauz, C. Wandrey, *Org. Process Res. Dev.* **2001**, *5*, 241 – 248.
[6] For representative recent reviews and books on organocatalysis see: a) J. Alemán, S. Cabrera, *Chem. Soc. Rev.* **2013**, *42*, 774 – 793; b) K. L. Jensen, G. Dickmeiss, H. Jiang, L. Albrecht, K. A. Jørgensen, *Acc. Chem. Res.* **2012**, *45*, 248 – 264; c) H. Pellissier in *Recent Developments in Asymmetric Organocatalysis*, RSC, Cambridge, **2010**; d) Organocatalysis thematic issue, *Chem. Rev.* **2007**, *107*, 5413 – 5883; e) *Enantioselective Organocatalysis, Reactions and Experimental Procedures* (Ed.: P. I. Dalko), Wiley-VCH, Weinheim, **2007**; f) B. List, *Acc. Chem. Res.* **2004**, *37*, 548 – 557; g) W. Notz, F. Tanaka, C. F. Barbas III, *Acc. Chem. Res.* **2004**, *37*, 580 – 591. For seminal papers see:h) K. A. Ahrendt, C. J. Borths, D. W. C. MacMillan, *J. Am. Chem. Soc.* **2000**, *122*, 4243 – 4244; i) B. List, R. A. Lerner, C. F. Barbas III, *J. Am. Chem. Soc.* **2000**, *122*, 2395 – 2396.
[7] a) N. Mase, C. F. Barbas III, *Org. Biomol. Chem.* **2010**, *8*, 4043 – 4050; b) C. F. Barbas III, A. Heine, G. Zhong, T. Hoffmann, S. Gramatikova, R. Björnestedt, B. List, J. Anderson, E. A. Stura, I. A. Wilson, R. A. Lerner, *Science* **1997**, *278*, 2085 – 2092.
[8] G. J. Bartlett, C. T. Porter, N. Borkakoti, J. M. Thornton, *J. Mol. Biol.* **2002**, *324*, 105 – 121.
[9] C. T. Porter, G. J. Bartlett, J. M. Thornton, *Nucleic Acids Res.* **2004**, *32*, 129D – 133D.
[10] a) K. Sharma, R. B. Sunoj, *Angew. Chem.* **2010**, *122*, 6517 – 6521; *Angew. Chem. Int. Ed.* **2010**, *49*, 6373 – 6377; b) M. B. Schmid, K. Zeitler, R. M. Gschwind, *Angew. Chem.* **2010**, *122*, 5117 – 5123; *Angew. Chem. Int. Ed.* **2010**, *49*, 4997 – 5003; c) M. J. Ajitha, C. H. Suresh, *J. Mol. Catal. A-Chem.* **2011**, *345*, 37 – 43; d) M. B. Schmid, K. Zeitler, R. M. Gschwind, *J. Org. Chem.* **2011**, *76*, 3005 – 3015.
[11] a) F. Giacalone, M. Gruttadauria, P. Agrigento, R. Noto, *Chem. Soc. Rev.* **2012**, *41*, 2406 – 2447; b) B. M. Trost, C. S. Brindle, *Chem. Soc. Rev.* **2010**, *39*, 1600 – 1632; c) S. Mukherjee, J. W. Yang, S. Hoffmann, B. List, *Chem. Rev.* **2007**, *107*, 5471 – 5569.
[12] S. Aratake, T. Itoh, T. Okano, N. Nagae, T. Sumiya, M. Shoji, Y. Hayashi, *Chem. Eur. J.* **2007**, *13*, 10246 – 10256.
[13] L. Q. Gu, M. L. Yu, X. Y. Wu, Y. Z. Zhang, G. Zhao, *Adv. Synth. Catal.* **2006**, *348*, 2223 – 2228.
[14] F. Giacalone, M. Gruttadauria, P. Agrigento, P. Lo Meo, R. Noto, *Eur. J. Org. Chem.* **2010**, 5696 – 5704.
[15] S. Guizzetti, M. Benaglia, L. Pignataro, A. Puglisi, *Tetrahedron: Asymmetry* **2006**, *17*, 2754 – 2760.
[16] X. H. Chen, S. W. Luo, Z. Tang, L. F. Cun, A. Q. Mi, Y. Z. Jiang, L. Z. Gong, *Chem. Eur. J.* **2007**, *13*, 689 – 701.
[17] V. Maya, M. Raj, V. K. Singh, *Org. Lett.* **2007**, *9*, 2593 – 2595.
[18] M. Lombardo, C. Trombini, *ChemCatChem* **2010**, *2*, 135 – 145 and references therein.
[19] A. Warshel, P. K. Sharma, M. Kato, Y. Xiang, H. Liu, M. H. M. Olsson, *Chem. Rev.* **2006**, *106*, 3210 – 3235.
[20] a) E. Montroni, S. P. Sanap, M. Lombardo, A. Quintavalla, C. Trombini, D. D. Dhavale, *Adv. Synth. Catal.* **2011**, *353*, 3234 – 3240; b) M. Lombardo, S. Easwar, F. Pasi, C. Trombini, *Adv. Synth. Catal.* **2009**, *351*, 276 – 282; c) M. Lombardo, M. Chiarucci, A. Quintavalla, C. Trombini, *Adv. Synth. Catal.* **2009**, *351*, 2801 – 2806; d) M. Lombardo, F. Pasi, S. Easwar, C. Trombini, *Synlett* **2008**, 2471 – 2474; e) M. Lombardo, S. Easwar, A. De Marco, F. Pasi, C. Trombini, *Org. Biomol. Chem.* **2008**, *6*, 4224 – 4229; f) M. Lombardo, F. Pasi, S. Easwar, C. Trombini, *Adv. Synth. Catal.* **2007**, *349*, 2061 – 2065.
[21] a) B. Ni, A. D. Headley, *Chem. Eur. J.* **2010**, *16*, 4426 – 4436; b) W. Miao, T. H. Chan, *Adv. Synth. Catal.* **2006**, *348*, 1711 – 1718; c) L. Zhou, L. Wang, *Chem. Lett.* **2007**, *36*, 628 – 629; d) D. E. Siyutkin, A. S. Kucherenko, M. I. Struchkova, S. G. Zlotin, *Tetrahedron Lett.* **2008**, *49*, 1212 – 1216; e) D. E. Siyutkin, A. S. Kucherenko, S. G. Zlotin, *Tetrahedron* **2009**, *65*, 1366 – 1372.
[22] N. Noujeim, L. Leclercq, A. R. Schmitzer, *Curr. Org. Chem.* **2010**, *14*, 1500 – 1516.
[23] M. Gruttadauria, F. Giacalone, R. Noto, *Adv. Synth. Catal.* **2009**, *351*, 33 – 57.
[24] N. Zotova, A. Franzke, A. Armstrong, D. G. Blackmond, *J. Am. Chem. Soc.* **2007**, *129*, 15100 – 15101.
[25] a) A. Fu, C. Zhao, H. Li, F. Tian, S. Yuan, Y. Duan, Z. Wang, *J. Phys. Chem. A* **2013**, *117*, 2862 – 2872; b) P. H.-Y. Cheong, C. Y. Legault, J. M. Um, N. Çelebi-Öülçum, K. N. Houk, *Chem. Rev.* **2011**, *111*, 5042 – 5137; c) D. Seebach, A. K. Beck, D. M. Badine, M. Limbach, A. Eschenmoser, A. M. Treasurywala, R. Hobi, *Helv. Chim. Acta* **2007**, *90*, 425 – 471.
[26] M. D. Prasanna, T. N. Guru Row, *Cryst. Eng.* **2000**, *3*, 135 – 154.
[27] A. R. Choudhury, U. K. Urs, T. N. Guru Row, K. Nagarajan, *J. Mol. Struct.* **2002**, *605*, 71 – 77.
[28] F. Giacalone, M. Gruttadauria, P. Lo Meo, S. Riela, R. Noto, *Adv. Synth. Catal.* **2008**, *350*, 2747 – 2760.
[29] Gaussian 09 (Revision A.02), M. J. Frisch, G. W. Trucks, H. B. Schlegel, G. E. Scuseria, M. A. Robb, J. R. Cheeseman, G. Scalmani, V. Barone, B. Mennucci, G. A. Petersson, H. Nakatsuji, M. Caricato, X. Li, H. P. Hratchian, A. F. Izmaylov, J. Bloino, G. Zheng, J. L. Sonnenberg, M. Hada, M. Ehara, K. Toyota, R. Fukuda, J. Hasegawa, M. Ishida, T. Nakajima, Y. Honda, O. Kitao, H. Nakai, T. Vreven, J. A. Montgomery, Jr., J. E. Peralta, F. Ogliaro, M. Bearpark, J. J. Heyd, E. Brothers, K. N. Kudin, V. N. Staroverov, R. Kobayashi, J. Normand, K. Raghavachari, A. Rendell, J. C. Burant, S. S. Iyengar, J. Tomasi, M. Cossi, N. Rega, J. M. Millam, M. Klene, J. E. Knox, J. B. Cross, V. Bakken, C. Adamo, J. Jaramillo, R. Gomperts, R. E. Stratmann, O. Yazyev, A. J. Austin, R. Cammi, C. Pomelli, J. W. Ochterski, R. L. Martin, K. Morokuma, V. G. Zakrzewski, G. A. Voth, P. Salvador, J. J. Dannenberg, S. Dapprich, A. D. Daniels, O. Farkas, J. B. Foresman, J. V. Ortiz, J. Cioslowski, D. J. Fox, Gaussian, Inc., Wallingford, CT, **2009**.
[30] a) Y. Zhao, D. G. Truhlar, *J. Phys. Chem. A* **2004**, *108*, 6908 – 6918; b) Y. Zhao, D. G. Truhlar, *J. Phys. Chem. A* **2005**, *109*, 5656 – 5667; c) Y. Zhao, D. G. Truhlar, *J. Phys. Chem. B* **2005**, *109*, 19046 – 19051; d) Y. Zhao, D. G. Truhlar, *Acc. Chem. Res.* **2008**, *41*, 157 – 167.
[31] N. Godbout, D. R. Salahub, J. Andzelm, E. Wimmer, *Can. J. Chem.* **1992**, *70*, 560 – 571.

Received: May 24, 2013
Published online on ■■ ■■, 0000

Stack attack! The asymmetric aldol reaction between cyclohexanone and benzaldehyde in the presence of tagged 4-hydroxy-prolines is modeled to elucidate the empirical concept of electrosteric activation, introduced to account for the much higher activity of *cis*-ion-tagged prolines. A complex interplay of hydrogen bonds and π-stacking interactions is found to give rise to the observed enhanced activity.

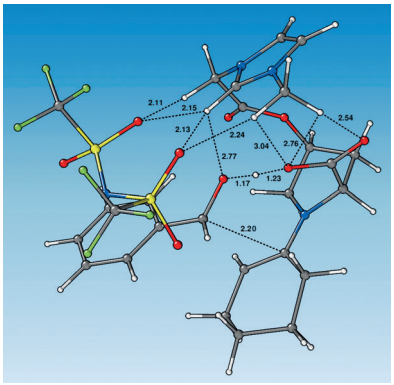

A. Bottoni, M. Lombardo, G. P. Miscione,* E. Montroni, A. Quintavalla, C. Trombini*

■■ – ■■

Electrosteric Activation by using Ion-Tagged Prolines: A Combined Experimental and Computational Investigation